

THERMAL CYCLING TESTING OF DISTRIBUTED FIBER OPTIC TEMPERATURE SENSORS FOR HIGH-TEMPERATURE APPLICATIONS

Darius D. Lisowski, Craig D. Gerardi, Steve W. Lomperski

Argonne National Laboratory

9700 South Cass Ave

Argonne, IL 60439-4840. USA.

dllisowski@anl.gov; cgerardi@anl.gov; lomperski@anl.gov

ABSTRACT

This paper describes thermal cycling tests of distributed fiber optic temperature sensors to characterize stability over a temperature range of 20 – 600°C. Stability and repeatability under thermal cycling are hallmarks of a reliable and useful thermometer. However, these critical performance characteristics are ill-defined for Rayleigh scattering-based distributed temperature sensors, especially for high-temperature service. For this study, eight sensors were placed in a small oven and cycled twenty-two times between ambient and staggered series of elevated temperatures. Sensor coatings were polyimide, gold, and CuBall copper alloy, along with two uncoated (bare glass) sensors. Uncoated sensors demonstrated the best stability with the least hysteresis. Polyimide-coated sensors exhibited a pronounced shift and hysteresis after an initial cycle, but stabilized for subsequent cycles as long as temperatures remained below the peak temperature of the initial cycle. The first cycle appears to “anneal” the coating by relieving residual strain. Metallic-coated sensors did not display this annealing behavior, exhibiting the most severe hysteresis and poorest repeatability of the samples tested. Though metallic coatings are intended to extend service temperature limits, the uncoated specimens not only performed better at high temperature but across the full range of studied temperatures.

KEYWORDS

Distributed fiber optic sensor, Rayleigh scattering, temperature sensor, coating, stability

1. INTRODUCTION

Distributed fiber optic sensors can map physical systems with data density well beyond the reach of conventional sensors. An entire fiber optic cable can serve as a sensor to provide thousands of measurements along a single optical fiber. They can be kilometers in length to map physical states of large structures or even terrain. For example, distributed fiber optic sensors have been deployed for temperature measurements within oil wells [1], along power cables serving offshore wind farms [2], and in the Dead Sea to characterize thermal stratification [3]. They also find use as strain sensors within infrastructure such as tunnels and pipelines [4] and textiles embedded within earthworks to monitor ground stability [5].

Applications in nuclear engineering can also benefit from the high data density available through distributed sensing with optical fiber. Such sensors have been used for sodium leak detection [6, 7], and are being tested for suitability in nuclear waste repositories [8] and as in-pile instrumentation [9]. They are also being incorporated into experiments in fluid mechanics [10, 11].

A variety of distributed sensing systems have been developed on the basis of Raman, Brillouin, and Rayleigh scattering. Our interest here is in temperature sensing based on Rayleigh scattering since the technique offers high spatial and temporal resolution suitable for fluid mechanics experiments used to validate computational fluid dynamics codes. Sensing systems can generate high resolution temperature data across a flow field without the need for chemical seeding, which is typically required of spectroscopic techniques such as laser-induced fluorescence. And unlike optical temperature measurement techniques, fiber optic sensors are suitable for applications that lack optical access or involve opaque fluids like liquid metals.

Though the Rayleigh scattering-based technique offers high spatial and temporal resolution, accuracy is not yet well defined, especially for high-temperature service. Previous studies have examined sensor operating temperature limits without considering repeatability [12] or given it only cursory consideration [13]. Though it is important to establish sensor operating range, measurement accuracy within the operating envelope must also be characterized if the sensor is to be of any practical use. One hallmark of a good temperature sensor is repeatability under thermal cycling with a lack of hysteresis. For this study we have placed eight sensors within a small oven for 22 thermal cycles between ambient and elevated temperatures, the maximum being 600°C for the final two cycles. Protective coatings on the fiber optic cables influence both service temperature limits and repeatability. Thus a variety of coating configurations were tested: polyimide, gold, and CuBall copper alloy, with two sensors uncoated (bare glass core inside a silica capillary). The next section briefly describes the measurement principle followed by experiment setup and test results.

2. SENSING PRINCIPLE

The distributed temperature sensors (DTS) examined in this study exploit the presence of Rayleigh scattering losses in fiber optic waveguides. Light is scattered by impurities and structural inhomogeneities at the molecular level, giving rise to a major source of signal loss in telecom fibers operating in the near infrared region. A small fraction of the loss is backscattered and available for analysis to interrogate the state of the optical fiber. The random distribution of inhomogeneities along a fiber core give rise to a backscatter pattern that is unique to the fiber and largely stable. The spectrum and amplitude of this pattern can be read to serve as a fiber signature. Physical changes such as strain and temperature shift the signature in a repeatable way, allowing the optical fiber to serve as a sensor.

A DTS system consists of an optical fiber, light source, detectors, and signal processing hardware (Figure 1). In a technique known as swept wavelength interferometry, a tunable laser launches a narrow band signal into the fiber for the purpose of registering resultant backscatter [14]. The scattering signal is mixed with a reference signal to generate an interference pattern for the detectors. The interference signal provides locations of scattering centers via Fourier transform into the frequency domain. The beat frequencies indicate relative position along the optical fiber with high frequencies at one end and low

frequencies at the other. Spatial resolution of the temperature/strain measurement is selected by inverse transformation of a narrow window of the spectrum. The window width determines the segment, or “gauge” length, of the DTS processed for each temperature/strain data point. For each measurement segment, backscatter amplitude as a function of wavelength is extracted from the test signal and cross correlated with the baseline signal. Shifts in the spectrum are proportional to strain and temperature changes from the baseline state.

Sensor response is described by that of a fiber Bragg grating, a forerunner of the distributed sensor. The wavelength shift is given by [14, 15]:

$$\frac{\Delta\lambda}{\lambda} = K_T\Delta T + K_\varepsilon\varepsilon \quad (1)$$

where K_T and K_ε are the temperature and strain coefficients, respectively. K_T includes coefficients for thermal expansion and the index of refraction. We are interested here in the temperature coefficient, which varies with composition and is on the order of $8 \times 10^{-6} \text{ K}^{-1}$ for silica fibers. This coefficient must be stable and invariant along the length of the optical fiber if it is to be a useful sensor. Note the differential nature of the measurement: a baseline is recorded and subsequent spectrum shifts indicate strain and/or temperature changes from the baseline state. Accuracy depends upon a stable baseline throughout a sensor’s designated operating range.

The sensing system used for this study is an ODiSI-B (Optical Distributed Sensor Interrogator) from Luna Inc., configured to use optical fibers up to 20 m in length at 5 mm spatial resolution and data rates to 50 Hz. Multiple fibers are multiplexed to the unit using a fiber optic switch. The measurement span was set to $\pm 75^\circ\text{C}$ providing temperature resolution of 0.1°C . Performance of the electronics is well characterized (0.8°C single scan repeatability for the configuration used here), but measurement accuracy ultimately depends primarily upon the sensor itself in conjunction with operating conditions.

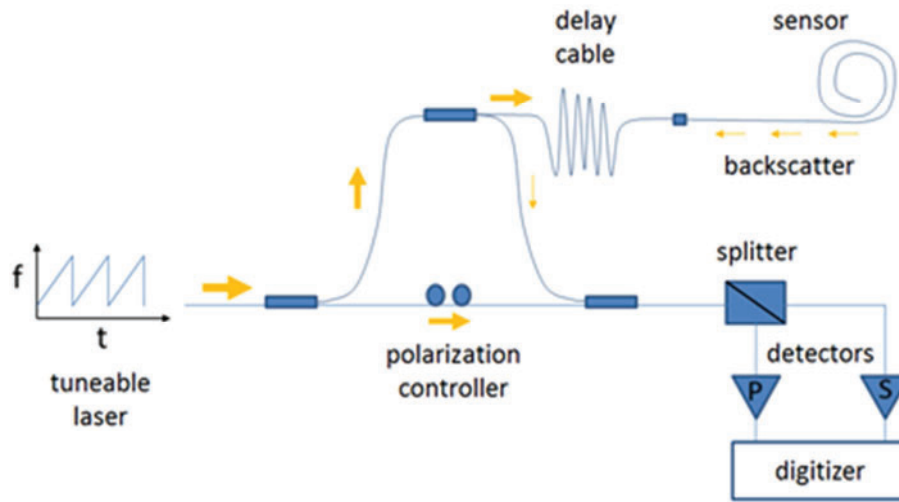


Figure 1: Principle components of a swept-wavelength interferometer for measuring Rayleigh backscatter

3. EXPERIMENT SETUP

Eight fibers were placed into a custom oven, constructed from copper tubing 12 mm in diameter and 300 mm long. The oven was heated by electrical resistance tape and insulated with a 50 mm thick layer of Kaowool blanket and enclosed in firebrick. Fibers passed completely through the oven with cold sections on each end. A thermocouple rake with nine K-type junctions was placed inside the oven alongside the fibers. Spacing between TC junctions is 25 mm. Oven temperatures were maintained by a PID temperature controller, and were repeatable within 2°C for oven set points < 350°C, and 4°C for set points > 350°C.

Three fibers were polyimide-coated (CL POLY 1310 21 NA Photonic), one gold-coated, two CuBall copper alloy, one bare fiber in a glass capillary, and the final fiber also bare but without the glass capillary. Each of the eight fibers was encased within its own 316 stainless steel capillary, gauge size 21RW (0.81mm OD, 0.5mm ID).

The region of interest for each fiber was limited to a 150 mm segment at the oven center, which provided temperatures across the center of the oven while omitting edge effects. At each oven setpoint fibers were polled 50 times at 5 Hz and temperatures determined using 5 mm gauge length and 2.5 mm spacing between data points.

3.1. Cycling Process

Data was generated by cycling the oven temperature to steady state set points (SP) and sampling data from both the K-type thermocouples and fibers. Each cycle began at room temperature followed by a series of 50°C increases to a predefined peak oven temperature. Cycles were then reversed, lowering temperature towards ambient with the same 50°C increments. The first half of a cycle with increasing temperature (heating) will be referred to as the “hot leg”, while the second half (cooling) back to ambient temperature is the “cold leg”.

The first cycle brought the oven SP to 200°C (Cycle 1) followed by eight cycles to a maximum of 150°C. Cycles 10-22 saw progressively higher peak oven temperatures ranging from 250 to 600°C (Figure 2). The inset table shows selected statistics for the test series: N_{samples} denotes the number of times at a particular SP, and is highest for low SPs since each cycle begins and ends near ambient temperature. There is only one ambient temperature measurement per cycle, taken at the beginning of the hot leg, and so N_{samples} at ambient temperature is only half that for 50°C, which has measurements for both the hot and cold legs. Uncertainty σ represents the standard deviation of average oven temperature across cycles at each SP, which provides an indication of repeatability of oven conditions at each SP. While thermocouple repeatability is better than 0.1°C, σ is considerably larger due to variations in soak time at each SP since the cycling process was not automated. The quantity σ represents a limit on our ability to assess fiber stability because sensors are expected to echo the oven temperature. Oven SP repeatability is superior at lower temperatures, e.g., 0.3°C at SP=50°C, and 4°C at 600°C.

The cycling sequence seen in Figure 2 was selected to examine potential annealing behavior of the coatings at $T_{oven} < 300^{\circ}\text{C}$. The first cycle was expected to exhibit significant offsets and/or hysteresis, followed by improved stability for subsequent cycles to a slightly lower peak temperature. The high temperature cycles in the second half of the test campaign were used to examine stability of the metal coated and bare fibers to assess their suitability for high-temperature service. In addition, this sequence allowed us to determine the effectiveness of burning off the polyimide coating in-situ to effectively create a bare sensor for high-temperature service.

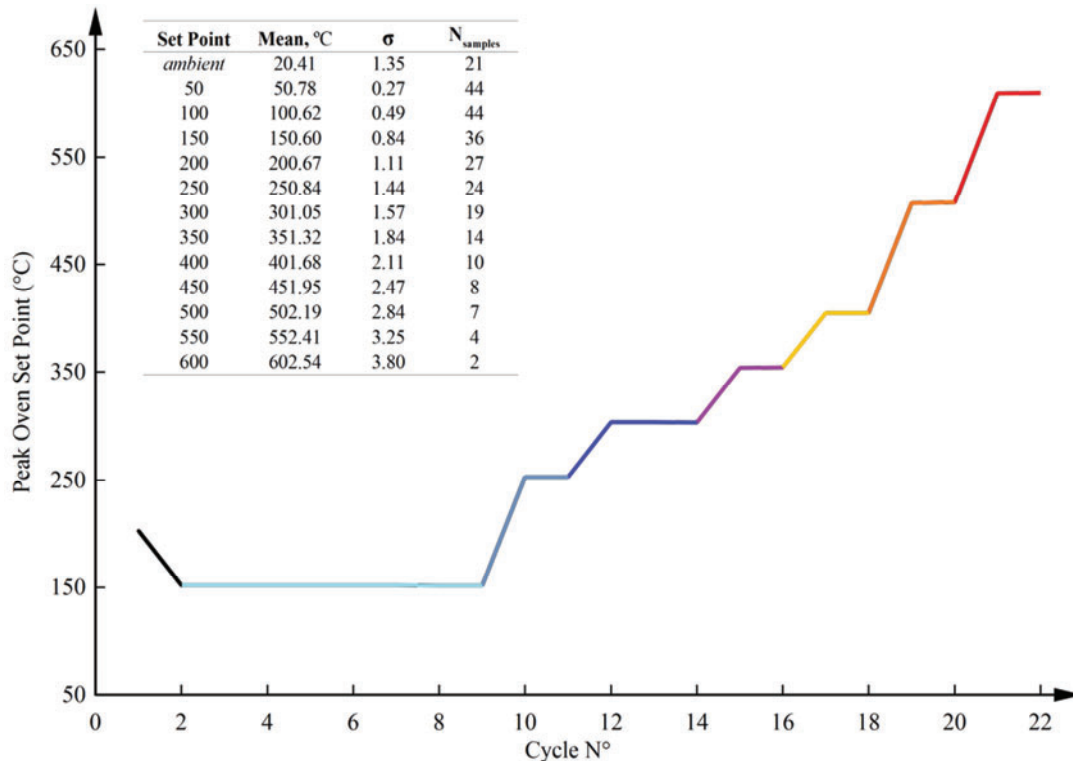


Figure 2: Peak oven temperature versus cycle number. Within each cycle oven temperature changed in 50°C increments. Inset indicates test campaign statistics: $N_{samples}$, total number of stops at each SP; σ , standard deviation in average oven temperature for $N_{samples}$

4. RESULTS

The benchmark for the following analysis is based on an average of six thermocouples within the oven, which span a distance of 150 mm within the 300 mm oven. All subsequent references to oven temperature correspond to this average. Figure 3 provides an illustration of the nature of raw fiber data and how it relates to the oven. The temperature distribution along a selected CuBall-coated fiber is plotted for a single cycle that began at ambient temperature and peaked at 400°C. Visible are the sections within the oven at elevated temperatures as well as exterior portions remaining at ambient temperature. Temperature gradients along the oven increase rapidly with temperature, which is expected for such a small system. Visible is the strain free entrance region ($x < 2.1\text{-m}$), the oven boundaries (2.2-m and 2.5-m), and strain free exit region ($x > 2.6\text{-m}$). Segments between the oven and strain free regions are subjected to high temperature gradients and strain and thus are omitted from the analysis. Figure 3 shows the region of interest (ROI) for the sensor, which is 150 mm of fiber near the center of the oven. In the analysis that follows, each fiber is represented by an average of 50 readings taken from the ROI.

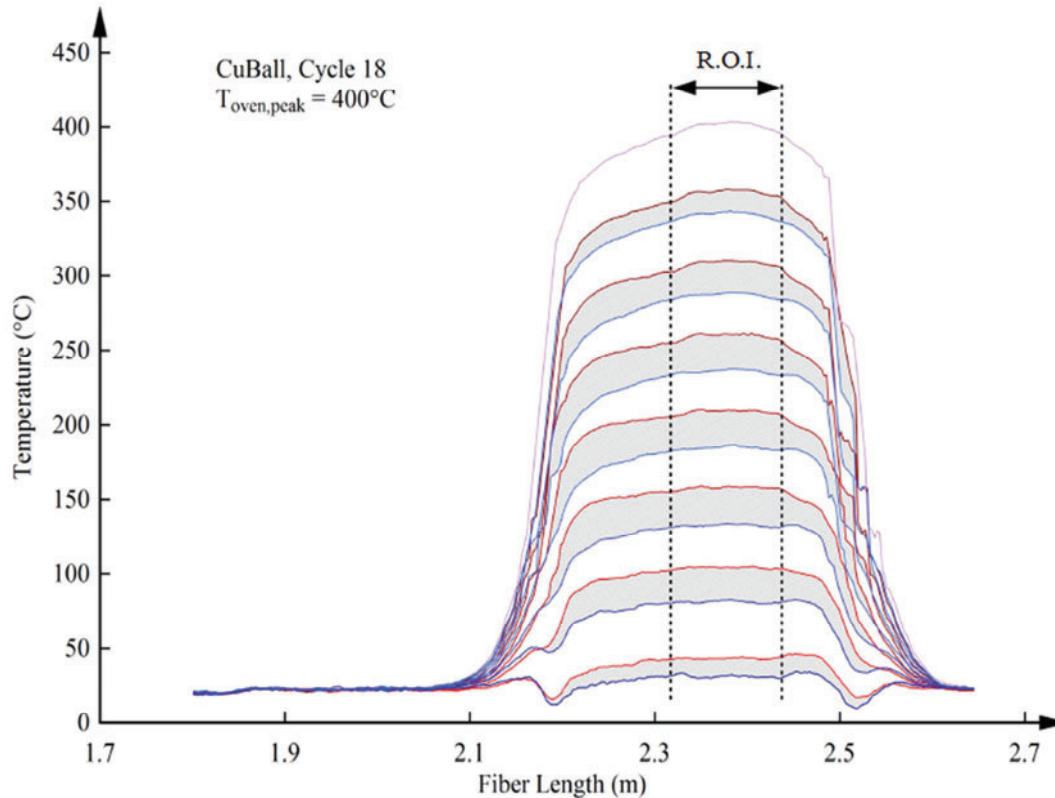


Figure 3: Cycle 18 data for selected fiber with Cuball coating. Shaded areas highlight hysteresis between hot and cold legs.

The areas shaded in grey highlight hysteresis between the hot and cold legs, which is more pronounced for the CuBall fibers than any of the other test subjects. Characterizing this type of shift for each fiber coating type is the primary focus here rather than sensitivity and calibration factors, which are known to vary with coating type [e.g., 11, 13]. Instead, this study examines stability of the calibration factor. Fiber optic cable can serve as a useful temperature sensor only if stability and hysteresis are within acceptable limits. And like conventional sensors, these performance characteristics are needed to establish measurement accuracy.

4.1. Cycling Shifts

Each cycle begins at ambient room temperature (nominally 20°C), stepped to the peak temperature set point in 50°C increments during the heat-up phase, and subsequently returned to 50°C in similar increments during the cool down phase. Thus, each fiber experienced a similar absolute oven temperature of twice within any given cycle. The difference in mean fiber temperature between the first 100°C (heating) and last 100°C (cooling) set point within a single cycle are shown in Figure 4.

Sensor stability and hysteresis are recognized as an important performance metrics and it is generally preferable to maximize the former and minimize the latter. We evaluated stability by subtracting fiber readings on the cold leg from those of the hot leg at the same SP.

$$\Delta T_{\text{Cycle N shift}} = T_{\text{Cycle N, 100°C, heating}} - T_{\text{Cycle N, 100°C, cooling}} \quad (2)$$

This figure of merit allows us to examine stability and hysteresis as a function of temperature and cycle number. For an ideal temperature sensor ΔT_{shift} would be identically zero for all SPs and cycles, and there would be no shaded regions such as those of Figure 3.

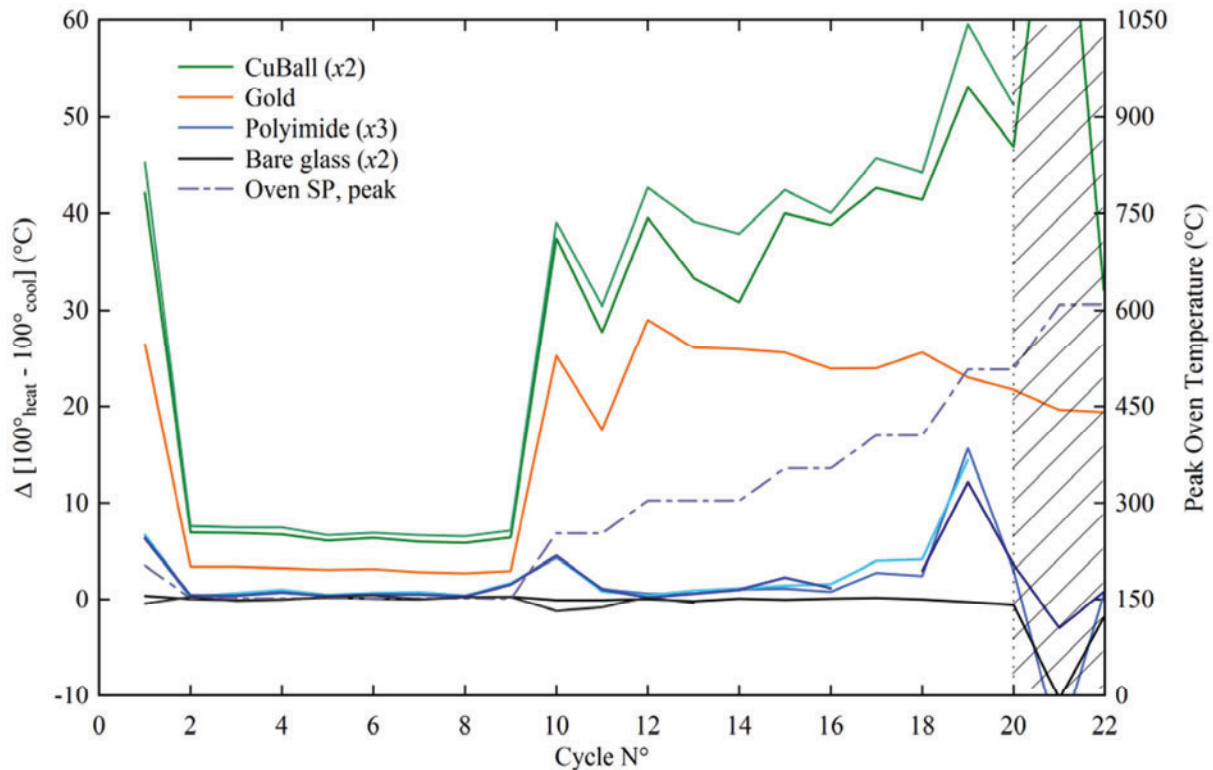


Figure 4: Temperature shift between the 100°C heat-up and cool down phases of each oven cycle. Shaded area on figure was performed near the dilatometric glass transition temperature of 600°C

The figure of merit ΔT_{shift} is plotted in Figure 4 over Cycles 1-10 for all fibers at an oven SP of 100°C. For Cycle 1, it is seen that ΔT_{shift} is $\geq 10^\circ\text{C}$ for all coated fibers. This means, specifically, that the average reading from the 150 mm ROI for the hot and cold legs differs by at least 10°C. In comparison, the average oven temperature as given by the thermocouples differed by only 0.6°C. This level of hysteresis is far beyond that observed in any thermocouple, which ranged from 3.24°C for polyimide to 15.19°C for CuBall. In contrast, ΔT_{shift} for the bare glass fiber is 0.39°C and within the repeatability of oven temperature as determined via the thermocouples.

The behavior of Cycles 2-9 is distinctly different from that of the first cycle. The quantity ΔT_{shift} is relatively stable for all coated fibers, and across these cycles shows a standard deviation averaging only 0.52°C. This suggests that some sort of ‘annealing’ process takes place when the sensors are first exposed to elevated temperatures. The annealing relieves residual strain that resides in the coating, after which the sensor shows improved repeatability as long as the service temperature does not exceed the annealing temperature. The coating is recognized as the object of the annealing process by noting the lack of this effect in the bare fiber, which remains stable across all cycles within 0.1°C.

4.2. Annealing Process

The initial cycling, or annealing process, is further explained in Figure 5, which outlines the fiber temperature during Cycles 1 – 3. During the first Cycle to a peak oven set point of 200°C, the fiber exhibits a well-defined offset between the heating and cooling curves, which for the Polyimide shown in Figure 5 was measured at 10.6°C. However as the cycle is repeated, the heating and cooling curves flatten onto each other and differ by only 1.1°C. This behavior is then continued for Cycle 3 and all subsequent cycles that are performed at peak oven temperatures equal or less than the first. If a new peak temperature is introduced, at a value greater than the first, this annealing process and curve shift is reintroduced.

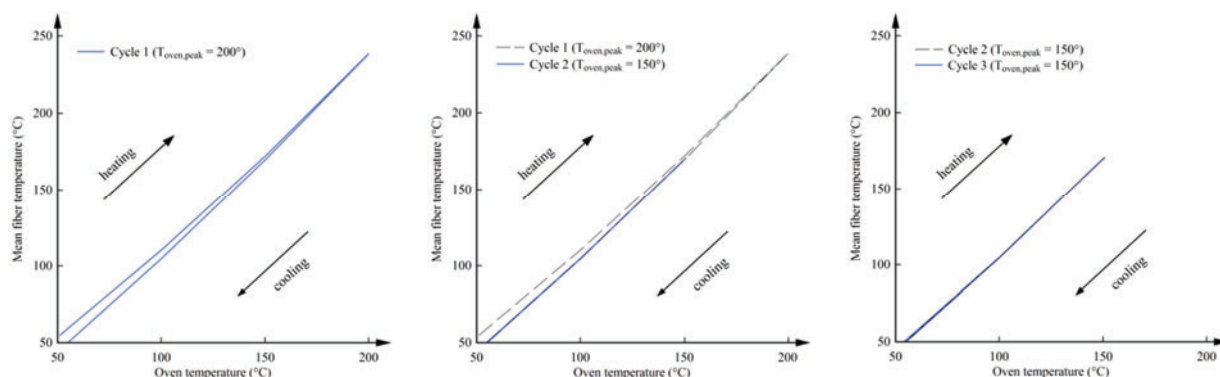


Figure 5: Cycling of Polyimide fiber detailing the annealing phenomenon

Among specific fibers, the bare glass is completely insensitive to this phenomenon and shows little to no annealing period. The polyimide exhibits a minor but significant annealing process that requires only a single cycle to complete, at which point the fiber returns to the previous, nominal temperature offset (1.32°C between Cycles 2 – 9). The metal-coated fibers, however, show an annealing process that is not satisfied by a single cycle – each new peak oven temperature raises the offset and remains nominally constant even after continued temperature cycles. While perhaps the gold-coated fiber shows signs of a long-term decay in temperature offset, the CuBall temperature offset continues to climb with each step elevation in peak oven temperature.

4.3. High Temperature Cycling

Peak oven temperature was incrementally raised through Cycles 10-22, repeating the peak temperature once or twice before increasing it for a subsequent cycle. This contrasts with the extended series of cycles to 150°C after the initial 200°C set point, which could have provided more support for the notion of annealing. But high-temperature behavior was also of interest while the allotted number of cycles for this study was limited. Still, the repetition of peak temperature reveals a few trends. Cycle 10, which increased peak temperature to 250°C for the first time, exhibits shifts in the opposite direction produced by the initial 200°C anneal. The trend is identical for all three coatings, which is remarkable since two are metal and one is a polymer. The return to 250°C in Cycle 12 shifts this temperature offset back towards the original level, again for all coating types. The same pattern is seen as the peak temperature is increased another 50°C to 300°C. Interestingly, the gold fiber exhibits a unique behavior after Cycle 17 –

even with further increases in absolute oven temperatures the measured error continues to fall. This perhaps suggest an ultimate annealing temperature specific to the gold fiber of 400°C, a finding that is of great interest and will be pursued in future studies.

Upon reaching Cycle 21, the mean oven temperature averaged near 600°C and introduced a new state for the fibers. This temperature is unique for glass (the core composition for all the fibers studied) as it approaches the dilatometric glass transition temperature of ~610°C [16]. At these extreme temperatures the glass structure is no longer well defined and begins a transition to a soft, rubber-like state. Thus, the cycling shifts began an erratic change that is unlike the behavior observed at lower temperatures. Among the four coating types cycled at 600°C, the glass experienced a shift of -10.2°C, CuBall +62.5°C, Polyimide -7.2°C, while the Gold remained near +9.1°C

We had anticipated a ‘burn-off’ behavior of the polyimide coating at these extreme temperatures, essentially reducing the fiber to that of a bare glass configuration. However this behavior was not observed at the temperatures studied in these tests. This burn-off may have occurred at the higher 600°C oven set points but will require additional cycling studies to fully characterize and will be the focus of future work.

4.4. Consistency along a distributed sensor

The major advantage of a fiber optic distributed sensor is that it provides many measurements along a single cable. Thus condensing data into averages, as in the preceding sections, omits a great deal of significant information. This has been done in the interest of clarity since it is easier to examine sensor stability at a single point or, as seen above, as an average over a ROI along the sensor. But to be useful as a distributed sensor, the fiber optic cable must have the same properties (sensitivity, repeatability, etc.) along its entire length. It would be difficult to make use of fibers requiring position-dependent calibrations. It is therefore of great interest to determine whether stability characteristics vary significantly with position. If so, it must be concluded that measurement accuracy would also vary with sensor position.

Thus, the local repeatability of each fiber is shown by a comparison of the heat-up and cool-down phases of each cycle to the first oven heat-up (cycle 1) for 100°C set points for Cycles 1 – 20 (Cycles 21 and 22 were omitted for clarity). This is presented by 2-dimension surface plots for each of the four coatings, Figure 6, where cycle number is plotted along the x-axis, physical fiber mapping along the y-axis, and a color band that represents the temperature offset at the respective location and cycle. Shown with identical temperature ranges for all coated fibers (bare glass is expanded in Figure 7 to emphasize low error ranges), the total error or temperature offset of the metal-coated fibers is readily apparent. Furthermore, the stark contrast between the local heat-up and cool down phases of the metal fibers is clearly portrayed by the alternating color bands. Finally, the annealing process is visible at new peak oven temperatures for both the metal and polyimide coated fibers, most apparent at the extreme set points of Cycles 2, 10, and 19 (150, 250, and 500°C, respectively).

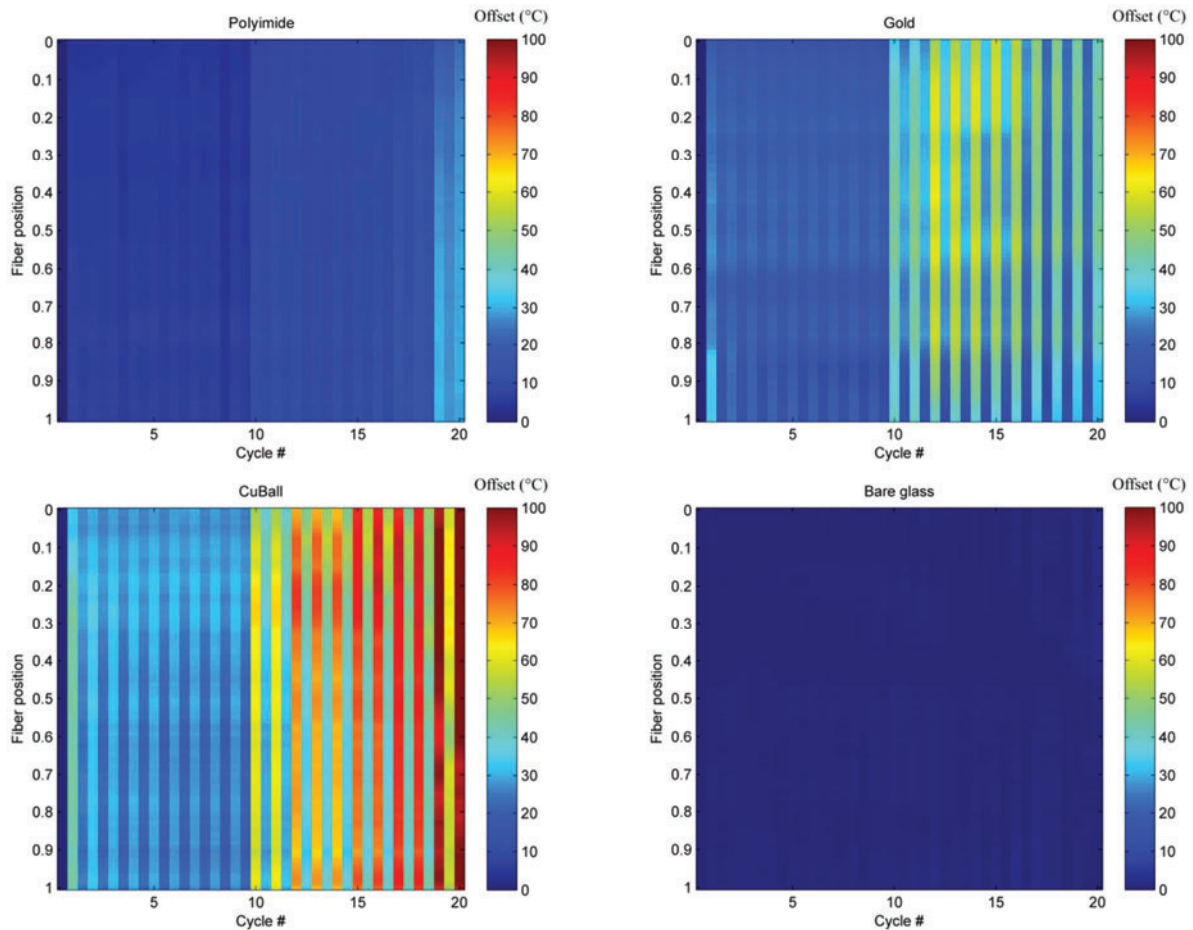


Figure 6: Plots of ΔT_{shift} at SP=100°C for four coatings. Each cycle includes both hot leg and cold leg data so that strong contrast in adjacent bands (gold & CuBall) indicates pronounced hysteresis.

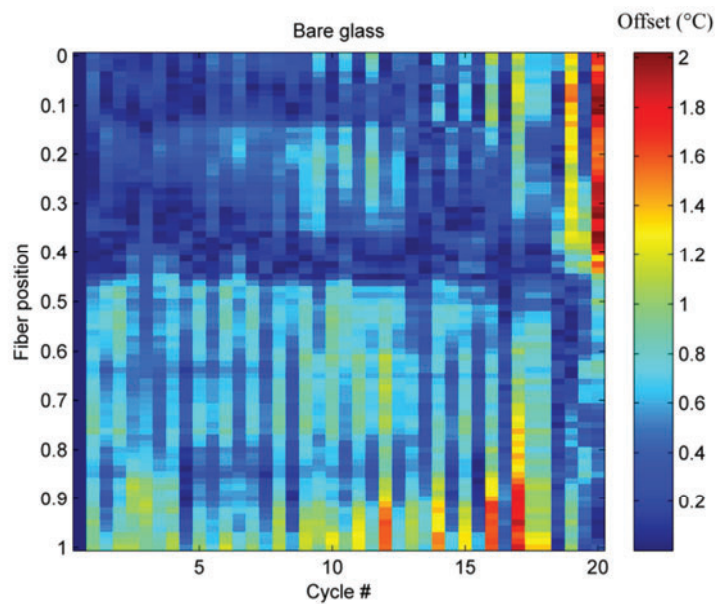


Figure 7: Expanded temperature scale of bare glass fiber from previous Figure 6

5. CONCLUSION

The bare glass fiber exhibited excellent repeatability with cycling errors of less than 0.1°C and was unperturbed by changes in peak cycle temperature. The coated fibers, however, exhibited hysteresis when introducing new peak oven temperatures. This effect was quickly attenuated for the polyimide fiber, which returned to its nominal error after a single cycle repeating the previous. This behavior we have coined the “annealing cycle”, and have found it to be a necessary step when utilizing coated fibers for temperature measurements. The metal coated fibers (CuBall, Gold), also exhibited signs of hysteresis however to a larger degree, and moreover a single annealing cycle was not satisfactory to reduce their error in any appreciable quantity. With each subsequent increase in peak oven temperature, the metal-coated fibers saw a deviation in their measured error for repeatability.

Thus if one wishes to obtain accurate and repeatable temperature measurements with polyimide fibers, an initial heat-up, or annealing cycle, is first necessary. Caution should be made when using metal coated fibers, such as CuBall or Gold, in the conditions presented in this manuscript as our results suggest poor repeatability and temperature performance. Further work is necessary to better understand the behavior of these metal coated fibers for DTS applications.

ACKNOWLEDGMENTS

This work was supported, in part, by the U.S. Department of Energy Office of Nuclear Energy, Office of Advanced Reactor Concepts under contract number DE-AC02-06CH11357.

REFERENCES

1. G. Williams, G. Brown, W. Hawthorne, A. Hartog, P. Waite “Distributed temperature sensing (DTS) to characterize the performance of producing oil wells,” *Proc SPIE 4202*, pp. 39-54 (2000).
2. M. Fromme, W. Christiansen, S. Kjaer, W. Hill, “Distributed temperature monitoring of long distance submarine cables”, *Proc. SPIE, Int Soc Opt Eng 7753 77532U:1-4* (2011).
3. A. Arnon, N.G. Lensky, J.S. Selker, “High-resolution temperature sensing in the Dead Sea using fiber optics”, *Water Resources Research*, **50**, pp. 1756-1772 (2014).
4. P. Rajeev, J. Kodikara, W.K. Chiu, T. Kuen, “Distributed optical fiber sensors and their applications in pipeline monitoring,” *Key Engineering Materials* **558**, pp. 424-434 (2013).
5. K. Krebber, P. Lenke, S. Liehr, N. Noether, M. Wendt, A. Wosniok, “Distributed fiber optic sensors embedded in technical textiles for structural health monitoring”, *Proc. SPIE 7653*, (2010).
6. M. Kasinathan, S. Sosamma, C. Babu Rao, Anish Kumar, B. Purna Chandra Rao, N. Murali, and T. Jayakumar, “Monitoring sodium circuits using fiber optic sensors”, *IEEE Transactions Nuclear Science*, **61**(4), pp. 1971-1976, (2014).
7. E. Boldyreva, R. Cotillard, G. Laffont, P. Ferdinand, D. Cambet, J.P. Jeannot, P. Charvet, G. Albaladéjo, Rodriguez, “Distributed temperature monitoring for liquid sodium leakage detection using OFDR-based Rayleigh backscattering”, *Proc. SPIE 9157*, 23rd International Conference on Optical Fibre Sensors, 91576N (2014).

8. X. Phéron, S. Girard, A. Boukenter, B. Brichard, S. Delepine-Lesoille, J. Bertrand, and Y. Ouerdane, "High γ -ray dose radiation effects on the performances of Brillouin scattering based optical fiber sensors," **Opt. Express** **20**, pp. 26978-26985 (2012).
9. C.M. Petrie, W. Windl, T.E. Blue, "In-situ reactor radiation-induced attenuation in sapphire optical fibers", *J. Am. Ceram. Soc.* **1**(7) (2014)
10. M. Weathered, M. Anderson, "Development of optical fiber sensors for use in sodium cooled reactor instrumentation", *Trans Amer Nuc Soc.* **111**, pp. 1623-1626 (2014)
11. S. Lomperski, C. Gerardi, W.D. Pointer, "Distributed fiber optic temperature sensor mapping of a jet-mixing flow field", *Exp. Fluids*, **55** (2015).
12. S. Sang, M. Froggatt, D. Gifford, S. Kreger, B. Dickerson, "One centimetre spatial resolution temperature measurements in a nuclear reactor using Rayleigh scatter in optical fiber", *IEEE Sensors Journal*, **8**, pp. 1375-1380 (2008).
13. S. Lomperski, C. Gerardi, D.W. Pointer, "Distributed fiber optic temperature sensing for CFD code validation", *15th Int Top Mtg Nuc Reactor Thermal Hydraulics*, NURETH-15, Pisa, Italy May 12-17 (2013).
14. D. Gifford, S. Kreger, A. Sang, M. Froggatt, R. Duncan, M. Wolfe, B. Soller, "Swept-wavelength interferometric interrogation of fiber Rayleigh scatter for distributed sensing", *Proc SPIE 6770*, Fiber Optic Sens and Appl V 67700F (2007).
15. K. Yüksel, P. Mégret, M. Wuilpart, "A quasi-distributed temperature sensor interrogated by optical frequency-domain reflectometer", *Meas. Sci. Technol.*, **22** (2011).
16. A. Karamanov, B. Dzhantov, M. Paganelli, D. Sighinolfi, "Glass transition temperature and activation energy of sintering by optical dilatometry", *Thermochimica Acta.*, **553**, pp. 1-7, (2013).